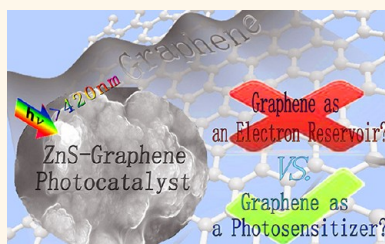


Graphene Transforms Wide Band Gap ZnS to a Visible Light Photocatalyst. The New Role of Graphene as a Macromolecular Photosensitizer

Yanhui Zhang,^{†,*} Nan Zhang,^{†,*} Zi-Rong Tang,[‡] and Yi-Jun Xu^{†,*,*}

[†]State Key Laboratory Breeding Base of Photocatalysis, College of Chemistry and Chemical Engineering, Fuzhou University, Fuzhou 350002, People's Republic of China and [‡]College of Chemistry and Chemical Engineering, New Campus, Fuzhou University, Fuzhou 350108, People's Republic of China

ABSTRACT We report the assembly of nanosized ZnS particles on the 2D platform of a graphene oxide (GO) sheet by a facile two-step wet chemistry process, during which the reduced graphene oxide (RGO, also called GR) and the intimate interfacial contact between ZnS nanoparticles and the GR sheet are achieved simultaneously. The ZnS–GR nanocomposites exhibit visible light photoactivity toward aerobic selective oxidation of alcohols and epoxidation of alkenes under ambient conditions. In terms of structure–photoactivity correlation analysis, we for the first time propose a new photocatalytic mechanism where the role of GR in the ZnS–GR nanocomposites acts as an organic dye-like macromolecular “photosensitizer” for ZnS instead of an electron reservoir. This novel photocatalytic mechanism is distinctly different from all previous research on GR–semiconductor photocatalysts, for which GR is claimed to behave as an electron reservoir to capture/shuttle the electrons photogenerated from the semiconductor. This new concept of the reaction mechanism in graphene–semiconductor photocatalysts could provide a new train of thought on designing GR-based composite photocatalysts for targeting applications in solar energy conversion, promoting our in-depth thinking on the microscopic charge carrier transfer pathway connected to the interface between the GR and the semiconductor.



KEYWORDS: graphene · ZnS · nanocomposite · photosensitizer · selective oxidation

Recently, graphene (GR)-based semiconductor photocatalysts have attracted a lot of attention because of their promising potential for conversion of solar to chemical energy.^{1–6} So far, GR-based semiconductor nanocomposite photocatalysts are mainly focused on “nonselective” degradation of pollutants (dyes, bacteria, and volatile organic pollutant) and water splitting to H₂.^{1–18} In contrast, research works on utilizing GR-based semiconductor nanocomposites for photocatalytic “selective” redox reaction are relatively limited. Recently, our group has reported GR–TiO₂ photocatalysts featuring an intimate interfacial contact that can be used as a visible light photocatalyst for selective oxidation of alcohols to corresponding aldehydes.^{19,20} On the other hand, GR–TiO₂ nanocomposites have been demonstrated to exhibit much higher photocatalytic activity than bare TiO₂ for selective photoreduction of CO₂ to CH₄ under both UV light and visible light irradiation.^{21,22} These research works highlight that, in addition to

the photocatalytic applications in environmental remediation and water splitting, there is a wide promising scope to exploit the potential applications of GR-based semiconductor nanocomposites in heterogeneous photocatalytic selective redox transformation under ambient conditions.

Notably, for the GR–semiconductor (*e.g.*, TiO₂, ZnO, CdS, ZnS, BiVO₄, WO₃, SnO₂, MnFe₂O₄, BiOBr, Bi₂WO₆, Sr₂Ta₂O₇, ZnSe) nanocomposites for photocatalytic applications available in literature,^{1–18,23–37} there seems to be a consensus that the photoactivity enhancement of the semiconductor after coupling with GR is attributed to the excellent electron conductivity of GR which acts as a 2D network of an electron reservoir to accept and shuttle electrons photogenerated from the semiconductor; as a result, the separation and lifetime of electron–hole pairs are prolonged, which thus contributes to the semiconductor photoactivity enhancement. On the other hand, we note that recent large-scale density functional

* Address correspondence to yjxu@fzu.edu.cn.

Received for review July 20, 2012 and accepted October 29, 2012.

Published online October 29, 2012
10.1021/nn304154s

© 2012 American Chemical Society

calculations on the model of the GR/TiO₂(110) interface, along with the experimental proof from the wavelength-dependent photocurrent study, have suggested the possible role of GR as a photosensitizer for TiO₂.³⁸ However, direct and robust experimental evidence on GR being a photosensitizer for semiconductors toward photocatalytic applications is unavailable. Furthermore, experimentally, only the photocurrent measurement cannot be sufficient enough to prove whether or not GR acts as a photosensitizer for a semiconductor during a photocatalytic process. An ideal choice to deeply explore this issue in this respect is to construct a GR–semiconductor hybrid nanocomposite along with a specific photoactivity test and analysis of the underlying photocatalytic reaction mechanism, during which the semiconductor is not able to be band-gap-photoexcited under visible light irradiation while, under this circumstance, the role of GR is able to be adequately investigated.

Herein, we have prepared the ZnS–GR nanocomposites featuring a good interfacial contact *via* a simple two-step wet chemistry approach. It is found that the addition of GR cannot sufficiently narrow the band gap of ZnS to the visible light region. However, the ZnS–GR nanocomposites do exhibit visible light photoactivity toward selective oxidation of alcohols and alkenes under ambient conditions. The structure–photoactivity correlation and reaction mechanism study using different radical scavengers reveal that the role of GR in the ZnS–GR nanocomposites is to act as a macromolecular organic dye-like photosensitizer, with which the photogenerated electrons from GR upon visible light irradiation can transfer to the conduction band of ZnS while ZnS by itself is not band-gap-photoexcited. The photosensitization process of ZnS by GR transforms the wide band gap ZnS semiconductor to exhibit the visible light photoactivity toward selective oxidation of alcohols and alkenes. This phenomenon is very similar to the photosensitization process of semiconductors by selective adsorption of organic dyes, for which the positive photogenerated holes from semiconductors do not

involve the photocatalytic process under visible light irradiation. Such a photocatalytic mechanism is distinctly different from all other GR–semiconductor photocatalysts available to date in literature,^{1–37} for which GR is always proposed to behave as an electron reservoir to capture or shuttle photogenerated electrons from the semiconductor upon light irradiation rather than the photosensitizing semiconductor. Therefore, our findings of such a novel photocatalytic reaction mechanism may provide a new train of thought on designing GR–semiconductor photocatalysts for conversion of solar to chemical energy toward target applications.

RESULTS AND DISCUSSION

The ZnS–GR nanocomposites have been fabricated *via* a two-step process in a solution phase. First, the ZnS ingredient is loaded onto GO by reaction of ZnCl₂ and Na₂S in a well-dispersed GO aqueous solution at room temperature. Subsequently, insulating GO is transformed to an electron-conducting GR by a well-established hydrothermal reduction treatment, while this step can also promote the interfacial interaction between ZnS and GR.^{8,9,19,20,39} Notably, GR prepared by the reduction of graphene oxide (GO, the precursor of GR) is widely adopted for synthesis of GR–semiconductor photocatalysts, also called reduced graphene oxide (RGO).^{1–37} Herein, for the convenience of comparison and discussion with graphene–semiconductor composite photocatalysts in the literature,^{1–37} the as-prepared nanocomposites are called ZnS–GR. The XRD patterns of GO, GR, and the resulting nanocomposites of ZnS–GR are shown in Figure 1. It can be seen that GO shows a sharp diffraction peak at 2θ value of *ca.* 10.1°. For the GR obtained from the hydrothermal reduction, the diffraction peak at *ca.* 10.1° disappears and a very broad diffraction peak at 2θ of *ca.* 25.0° appears, which means that GO sheets have been effectively exfoliated from the raw graphite and, after hydrothermal reduction, almost all GO sheets have been transformed to GR with a random packing and significantly less functionalities.^{8,9} For the ZnS–GR nanocomposites with different weight

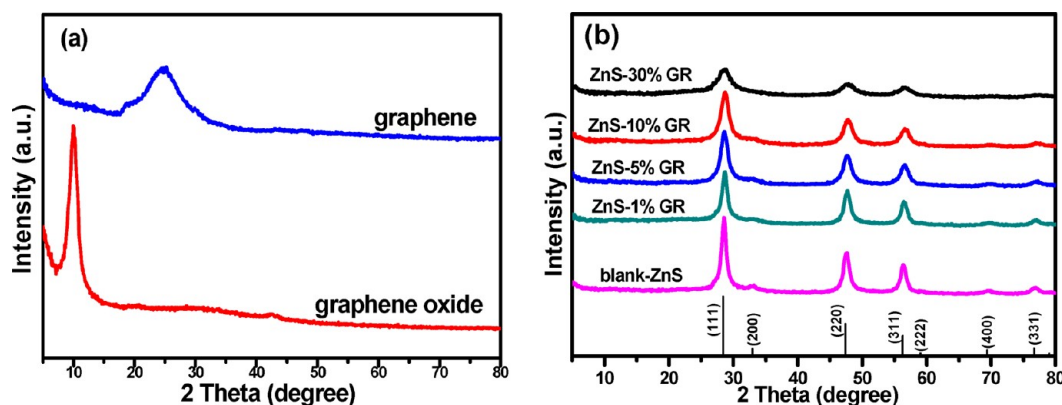


Figure 1. XRD patterns of the samples of GR and GO (a), and the samples of blank ZnS and ZnS–GR nanocomposites with different weight addition ratios of GR (b).

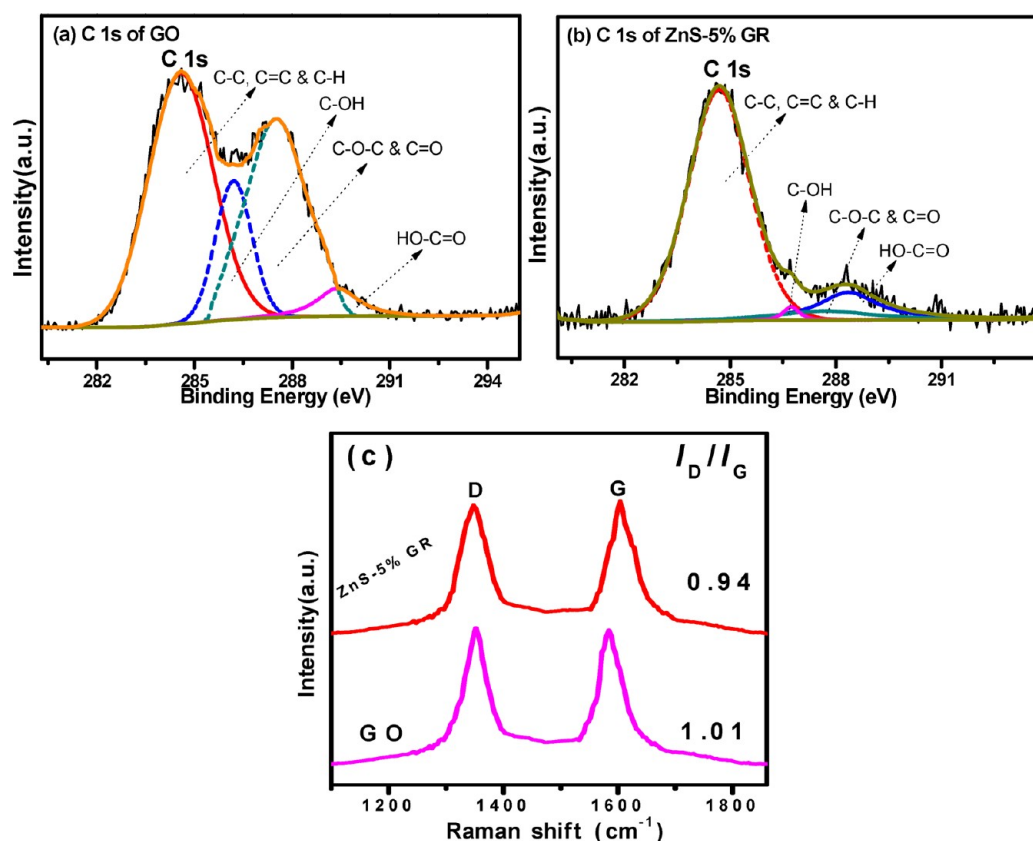


Figure 2. C 1s X-ray photoelectron spectra (XPS) of the original GO (a), ZnS–5%GR nanocomposite (b), and Raman spectra of the ZnS–5%GR nanocomposite and GO (c).

addition ratios of GR, they show similar XRD patterns with blank ZnS. The peaks located at *ca.* 28.5, 47.5, and 56.3° can be indexed to (111), (220), and (311) crystal planes of the face centered cubic (fcc) ZnS (JCPDS No. 05-0566).³⁷ Notably, no diffraction peaks for GR can be observed in the nanocomposites of ZnS–GR, which might be due to the low amount and relatively low diffraction intensity of GR in the nanocomposites of ZnS–GR.

The efficient reduction of GO to GR after the hydrothermal treatment can also be evidenced by the contrast comparison of the C 1s X-ray photoelectron spectra (XPS) of GO and ZnS–GR (here, taking ZnS–5% GR as an example), which is displayed in Figure 2a,b. For the bare GO, the C 1s XPS spectra suggest the abundance of various oxygen-containing functional groups on the GO surface. For the ZnS–5%GR nanocomposite, the significant loss of oxygen-containing functional groups is observed based on the C 1s XPS spectra in Figure 2b, which indicates the sufficient reduction of GO to GR after coupling ZnS with GO via a hydrothermal reduction treatment.^{19,40} The XPS result is in good agreement with the Fourier transformed infrared spectroscopy (FTIR), as shown in Figure S1 (Supporting Information). In addition, the carbon doping for ZnS is not observed from the XPS analysis. Figure 2c shows the Raman spectra of GO and the ZnS–5%GR nanocomposite. Of particular note is the

intensity ratio of the D and G bands, I_D/I_G , which is a measure of the relative concentration of local defects or disorders (particularly the sp^3 -hybridized defects) compared to the sp^2 -hybridized GR domains.^{19,21} It can be seen that the I_D/I_G ratio is 1.01 for GO. After the hydrothermal reaction, the I_D/I_G ratio is decreased to 0.94, thus indicating more graphitization of the ZnS–5%GR nanocomposite resulting from the hydrothermal reduction process.

We have also used the field-emission scanning electron microscopy (FESEM) to directly analyze the morphology of the ZnS–5%GR nanocomposite. It can be observed from Figure 3c,d that ZnS particles spread uniformly on the surface of GR nanosheets, and the two-dimensional (2D) structure of GR sheets with micrometers-long wrinkles can be clearly distinguished. There is an intimate interfacial contact between GR and ZnS particles. To further obtain the microscopic morphology and structure information, the transmission electron microscopy (TEM) analysis of ZnS–5%GR has been performed, as shown in Figure 4. It can be seen from Figure 4a–c that there is a nice dispersion of nanosized ZnS particles on the surface of the GR sheet support. Three distinct diffraction rings are seen from the selected area electron diffraction (SAED) pattern in Figure 4d, which can be indexed to (111), (220), and (311) crystal planes of ZnS. Besides, the SAED pattern also indicates that the

ZnS–5%GR nanocomposite possesses a polycrystalline structure, which is in accordance with the result of XRD analysis. The joint SEM and TEM characterization suggests a good interfacial contact formed between the ZnS nanoparticles and the 2D GR sheet. Since the transfer process of charge carriers in GR–semiconductor nanocomposites is intimately related with the interfacial interaction between GR and the semiconductor,^{19–37} it could be expected that such a good interfacial contact for the ZnS–5%GR nanocomposite should favor the charge carrier transfer process.

It is well-known that ZnS with a cubic form is a wide band gap (*ca.* 3.60 eV) semiconductor,³⁷ with which it cannot be band-gap-photoexcited by visible light irradiation. For the GR–semiconductor nanocomposites,

it has been demonstrated that the band gap of the semiconductor, such as TiO₂, can be narrowed to the visible light region resulting from the chemical bonding between GR and the semiconductor.^{8,9,11,16,19} As a result, GR–TiO₂ can exhibit visible light photoactivity. Such a similar phenomenon of band gap narrowing has also been observed for our ZnS–GR nanocomposites, which is reflected by the optical property measurements of ZnS–GR nanocomposites, using the UV–vis diffuse reflectance spectra (DRS), as shown in Figure 5a. It can be seen that the addition of different amounts of GR affects the optical property of light absorption for GR–ZnS nanocomposites significantly. With the increase of GR content, there is an enhanced absorbance in the visible light region ranging from 400 to 800 nm, which is in accordance with the color change of the samples (Figure S2, Supporting Information). A plot obtained *via* the transformation based on the Kubelka–Munk function *versus* the energy of light is shown in Figure 5b, from which the rough band gap values of the samples are estimated to be 3.55, 3.52, 3.45, and 3.44 eV corresponding to blank ZnS, ZnS–1%GR, ZnS–5%GR, and ZnS–10%GR, respectively. This result indicates a band gap narrowing of the semiconductor ZnS due to the coupling in GR–ZnS nanocomposites. However, it should be noted that, for ZnS–30%GR, it is difficult to determine the exact band gap value because the much higher weight addition of GR leads to a very significant background absorption ranging from 400 to 800 nm, as also observed for TiO₂–GR photocatalysts with higher weight addition ratios of GR.¹⁹

The above optical measurement of ZnS–GR indicates that the wide band gap of ZnS is narrowed to some degree, but still not enough to the visible light region. Thus, in principle, both blank ZnS and ZnS–GR

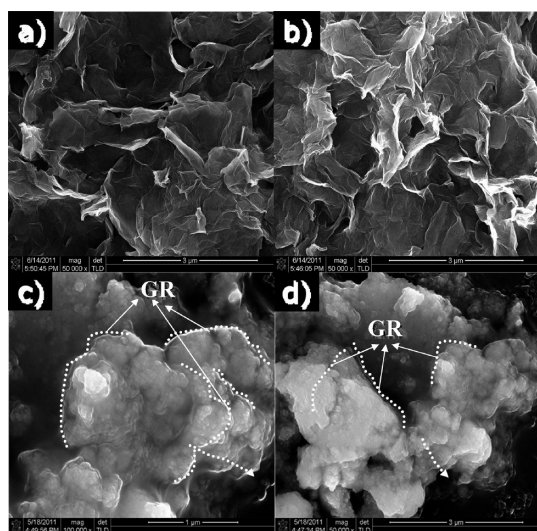


Figure 3. Typical SEM images of GR (a,b) and ZnS–5%GR nanocomposite (c,d).

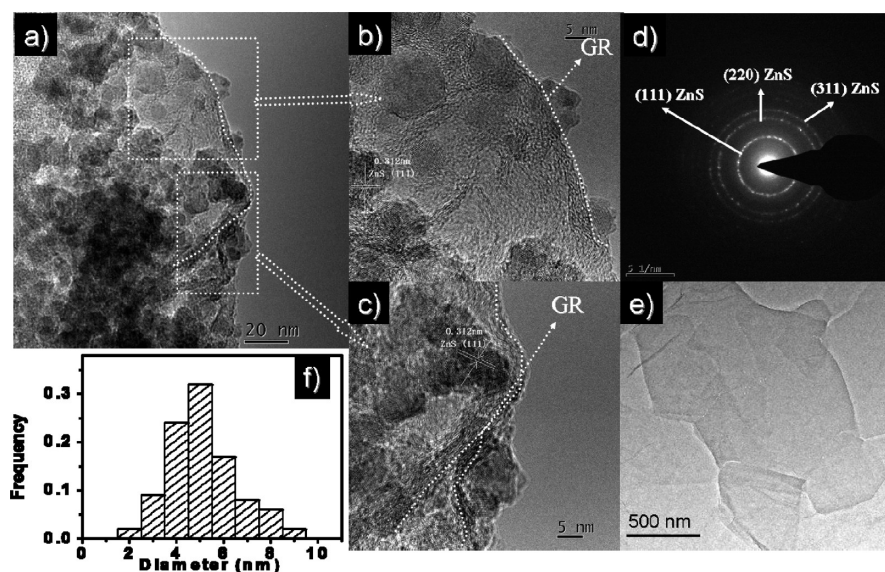


Figure 4. TEM image of ZnS–5%GR (a), high-resolution TEM (HRTEM) images of ZnS–5%GR (b,c), selected area electron diffraction (SAED) pattern of ZnS–5%GR (d), original bare GR sheet (e), and size distribution of ZnS nanoparticles in ZnS–5%GR (f).

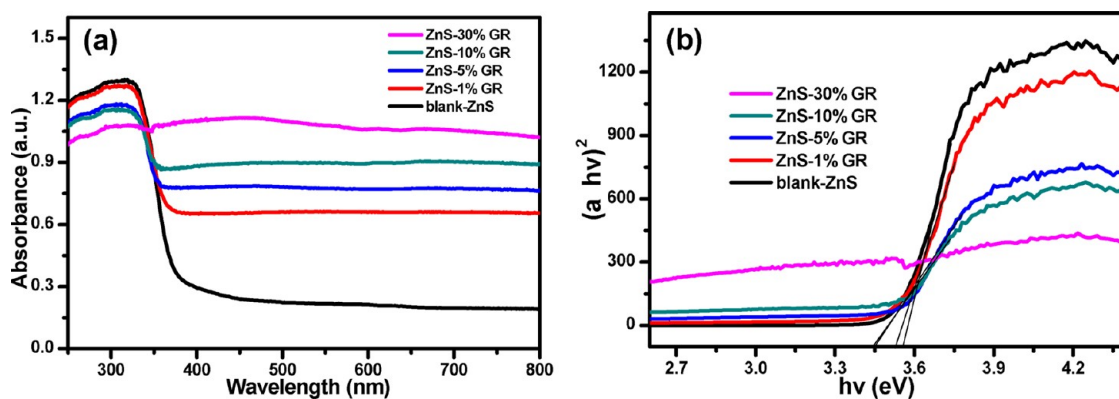


Figure 5. UV-visible diffuse reflectance spectra (DRS) of the samples of ZnS-GR nanocomposites with different weight addition ratios of GR and blank ZnS (a), and the plot of transformed Kubelka-Munk function versus the energy of light (b).

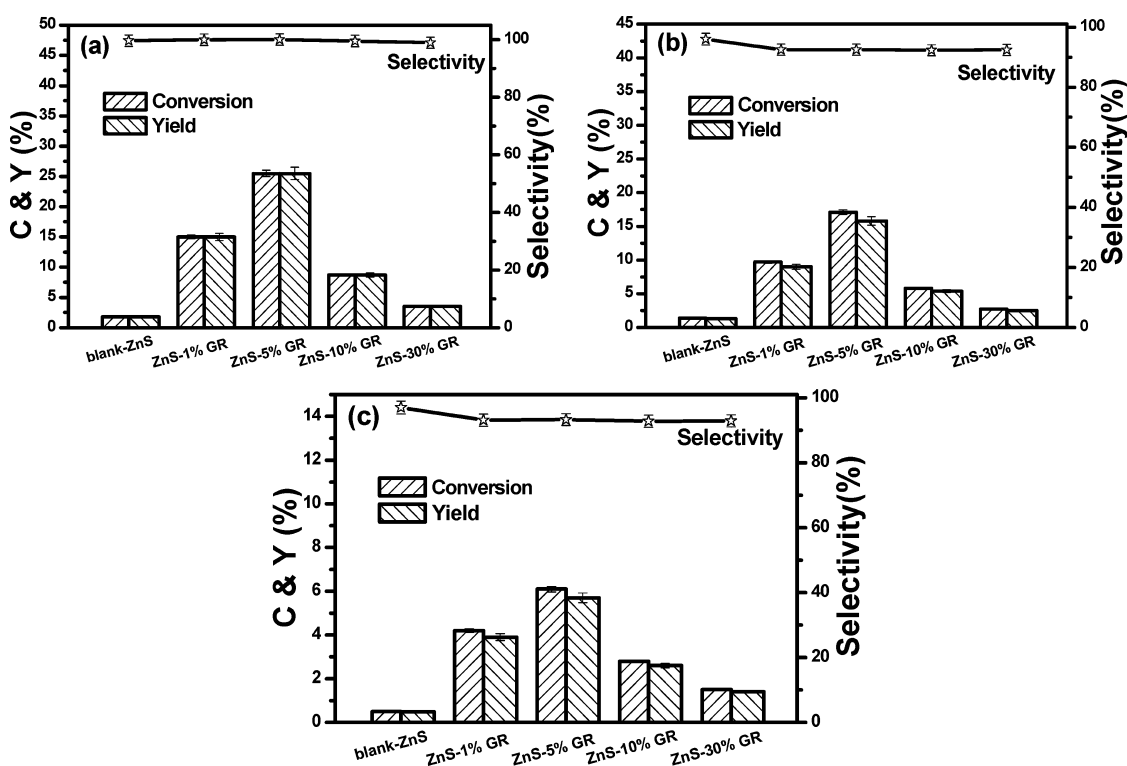


Figure 6. Results of photocatalytic selective oxidation of organic compounds over blank ZnS and ZnS-GR nanocomposites under visible light irradiation ($\lambda > 420$ nm) for 4 h; (a) benzyl alcohol; (b) 3-methylbut-2-en-1-ol; (c) styrene.

should not exhibit visible light photoactivity. However, when we perform the photocatalytic selective oxidation of alcohols and alkenes over GR-ZnS nanocomposites, we find that they do have visible-light-driven photoactivity ($\lambda > 420$ nm). As shown in Figure 6, ZnS-GR shows the photoactivity toward selective oxidation of benzyl alcohol and 3-methylbut-2-en-1-ol to corresponding aldehydes and selective oxidation of styrene to styrene oxide. In addition, in order to get a synergetic effect between ZnS and GR, it is crucial to control the addition ratios of GR, which thus leads to an optimum photoactivity. It is clear that the ZnS-5%GR nanocomposite exhibits the best visible light photocatalytic performance. Excessive addition of black color

GR will lower the light intensity through the depth of reaction solution, thus resulting in the decreased photoactivity.^{8,19-22} In contrast, blank ZnS shows very poor photoactivity. For example, after visible light irradiation for 4 h, 26% yield of benzaldehyde is reached over the photocatalyst of ZnS-5%GR, which is about 9 times higher than that over blank ZnS. The 6% yield of styrene oxide is obtained over ZnS-5%GR, which is about 6 times higher than that over blank ZnS. Importantly, when the visible light irradiation time is prolonged, we find that the conversion and yield over ZnS-5%GR are increased correspondingly, as shown in Figure 7. However, irradiation time plays a negligible effect on the very low conversion and yield over blank

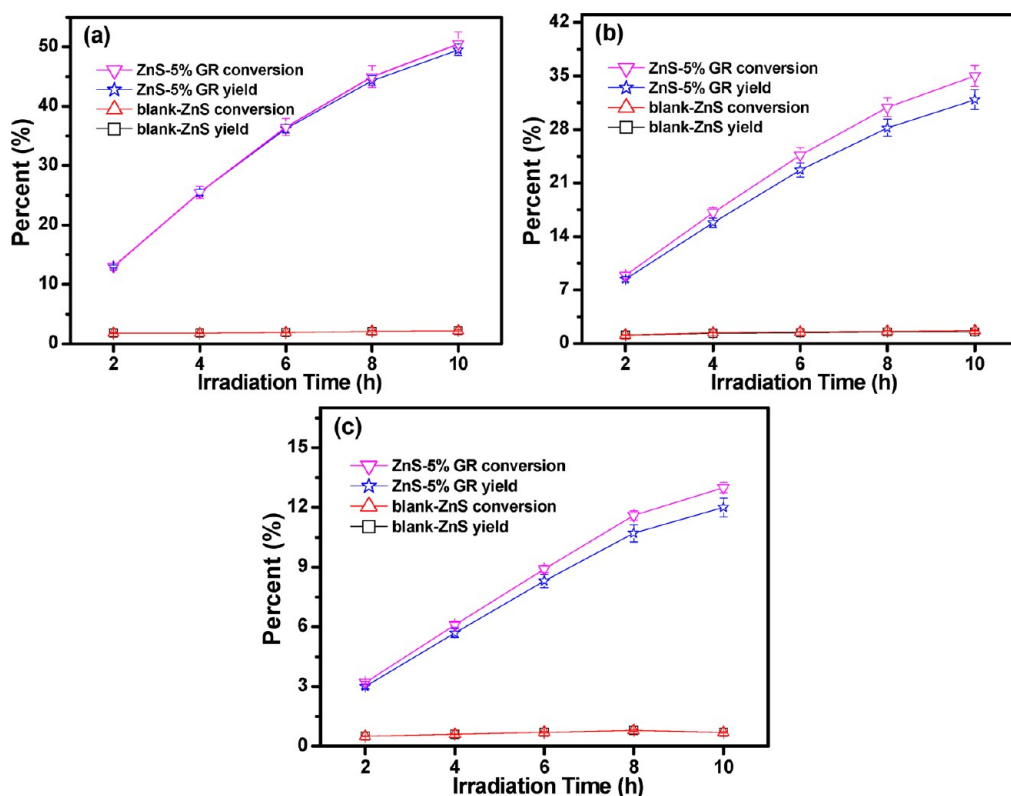


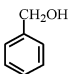
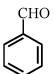
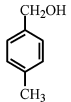
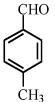
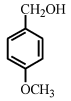
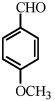
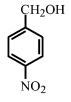
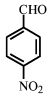
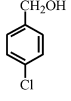
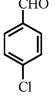
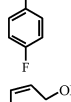
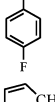
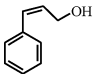
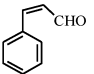
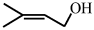
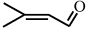
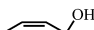
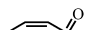
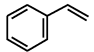
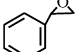
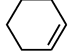

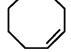
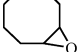
Figure 7. Results of time-online profiles of photocatalytic selective oxidation of organic compounds over blank ZnS and ZnS-5%GR under the irradiation of visible light ($\lambda > 420$ nm); (a) benzyl alcohol; (b) 3-methylbut-2-en-1-ol; (c) styrene.

ZnS, indicating that the slight conversion of substrate alcohol or alkene over blank ZnS cannot be attributed to a characteristic photocatalytic process. In addition, only the trace conversion is obtained using the bare GR, suggesting that GR by itself cannot directly act as visible light photocatalyst for selective oxidation of alcohol or alkene. On the contrary, the coupling of ZnS with GR plays a key role in tuning the visible-light-driven photoactivity of ZnS in the ZnS-GR nanocomposites. In addition to benzyl alcohol, 3-methylbut-2-en-1-ol, and styrene, we have also tested the photocatalytic performance of ZnS-5%GR toward selective oxidation of other alcohols and alkenes under visible light irradiation. The results after visible light irradiation for 10 h are listed in Table 1, from which it can be seen that ZnS-5%GR also has the visible light photoactivity toward various alcohols and alkenes. The selectivity to target products is in the range of 88–98%. Notably, photocatalytic selective epoxidation of alkenes is relatively more difficult compared to selective oxidation of alcohols over ZnS-5%GR under visible light irradiation, suggesting the easier oxidation of $-\text{CH}_2\text{OH}$ groups in alcohols as compared to $-\text{C}=\text{C}-$ groups in alkenes. Blank experiments in the absence of catalysts and/or visible light irradiation show no conversion of substrate reactants, which ensures that the reaction is really driven by a photocatalytic process.

As mentioned above, the addition of GR causes the band gap narrowing of ZnS to ca. 3.45 eV for ZnS-5%

GR. However, this band gap is still so large that visible light irradiation ($\lambda > 420$ nm) cannot photoexcite electrons in the valence band (VB) to conduction band (CB) of ZnS. Thus, GR must play a key role in making ZnS-5%GR have visible light photoactivity. From the previous photocatalysts of semiconductor- C_{60} and semiconductor-carbon nanotube (CNT),^{40,41} we could glean the possible hints to infer that GR acts as a visible light photosensitizer to ZnS in the nanocomposite of ZnS-5%GR. In other words, under visible light irradiation, photoexcited electrons are generated from GR and then transferred to the CB of ZnS, which therefore transforms wide band gap ZnS to a visible light photocatalyst. Such a similar photocatalytic reaction mechanism has been proposed in previous semiconductor- C_{60} or -CNT visible light photocatalysts.^{40–43} For example, Kamat *et al.* have found that, for the C_{60} - TiO_2 photocatalyst, C_{60} can be photoexcited under visible light laser beam irradiation, and the photoinduced electrons can be transferred to the CB of TiO_2 .⁴² Wang *et al.* once proposed that, for the CNT- TiO_2 photocatalyst, CNT might be a photosensitizer for TiO_2 ; under visible light irradiation, the photoinduced electrons from the CNT could be produced and transferred to the CB of TiO_2 .⁴³ However, this work does not exclude the effect if there is a Ti-O-C bond formed between TiO_2 and CNT, that is, surface carbon doping.^{40,43} Thus, the proposed role of the CNT as a photosensitizer for TiO_2 is just a possible speculation. Indeed, the

TABLE 1. Photocatalytic Selective Oxidation of Organic Compounds over the ZnS–5%GR Photocatalyst under the Irradiation of Visible Light ($\lambda > 420$ nm) for 10 Hours

Entry	Substrate	Product	Conversion (%)	Yield (%)	Selectivity (%)
1			51	50	98
2			50	48	96
3			54	53	98
4			37	36	96
5			46	45	98
6			45	43	96
7			43	38	89
8			35	32	91
9			33	30	92
10			13	12	92
11			9	8	91
12			10	9	88

CNT–TiO₂ photocatalytic mechanism proves to be a more complex problem.⁴⁰ The possible role of the CNT as a photosensitizer for semiconductors has not been well-understood, and it still remains a challenge.^{40,41} However, these chemical precedents promote us to envision that, for ZnS–5%GR photocatalyst, the role of GR could act as a macromolecular “photosensitizer” for ZnS, hence making it exhibit visible light photoactivity. This case is seemingly similar to the photosensitization process of semiconductors by selective matched adsorption of organic dyes, for which the positive photogenerated holes from semiconductors do not involve the photocatalytic process because of the inability of band

gap excitation of the semiconductor (*e.g.*, TiO₂) to generate electron–hole pairs under visible light irradiation.⁴⁴

The above inference on the role of GR as a macromolecular organic dye-like photosensitizer to ZnS for ZnS–5%GR can be supported by the controlled experiments using different radicals scavengers, which also help us understand the underlying photocatalytic mechanism.^{45–50} As shown in Figure 8, when the *tert*-butyl alcohol (TBA) scavenger for hydroxyl radicals is added, conversion of benzyl alcohol is almost unchanged. This is reasonable because, in the solvent of benzotrifluoride (BTF), no hydroxyl radicals are generated, whereas the superoxide radicals can be formed,^{19,20,45}

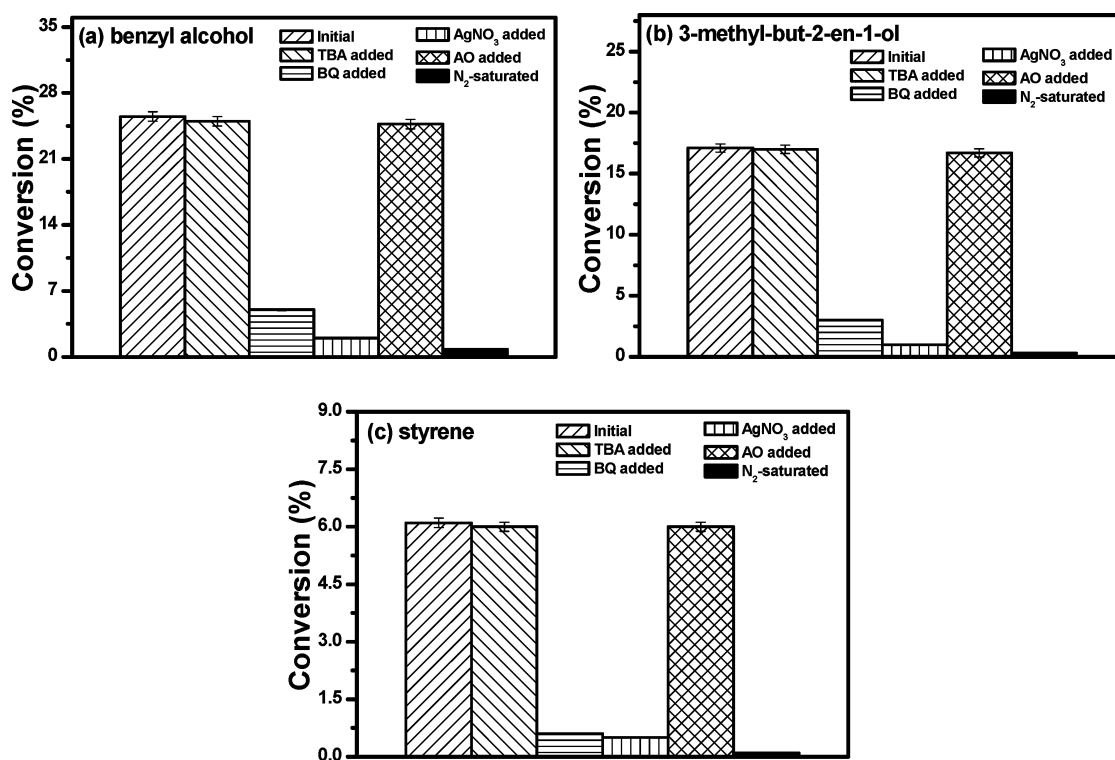


Figure 8. Controlled experiments of photocatalytic selective oxidation of benzyl alcohol (a), 3-methylbut-2-en-1-ol (b), and styrene (c) in the presence of *tert*-butyl alcohol (TBA, scavenger for hydroxyl radicals), benzoquinone (BQ, scavenger for superoxide radicals), AgNO₃ (scavenger for electrons), ammonium oxalate (AO, scavenger for holes), or N₂-saturated condition over the optimum ZnS–5%GR under visible light irradiation ($\lambda > 420$ nm) for 4 h.

which is confirmed by the electron spin resonance spectra (ESR) analysis on the suspension of ZnS–5%GR in BTF solvent, as shown in Figure S3 (Supporting Information). Furthermore, it should be mentioned that, over blank ZnS, no superoxide radicals are observed because the bare ZnS cannot be photoexcited due to its wide band gap. This suggests that the electrons are photogenerated from GR in ZnS–5%GR instead of ZnS, with which oxygen can be activated to give the formation of superoxide radical species. It is interesting to note that the addition of ammonium oxalate (AO) scavenger for holes has a negligible effect on conversion of substrate reactants, such as benzyl alcohol (a), 3-methylbut-2-en-1-ol (b), or styrene (c) (see Figure 8), thus indicating holes do not involve the oxidation of alcohol or alkene. This result is in accordance with the proposed photocatalytic mechanism that GR acts as a visible light photosensitizer in ZnS–5%GR during which no holes are generated because ZnS cannot be band-gap-photoexcited by visible light irradiation. When AgNO₃ scavenger for electrons is added, conversion of substrate reactants is remarkably inhibited. Similarly, the addition of benzoquinone (BQ) scavenger for superoxide radicals also significantly prohibits the conversion. Besides, controlled experiment in inert N₂-saturated atmosphere suggests that only trace conversion is obtained. Thus, these controlled experiments suggest that (i) oxygen is the primary oxidant in our photocatalytic oxidation

system, and (ii) photocatalytic oxidation of alcohols or alkenes over ZnS–5%GR under visible light irradiation can be understood by a GR-induced photosensitization process. The generation of photoexcited charge carriers for ZnS–5%GR under visible light irradiation is also confirmed by the measurement of photocurrent transient responses for ZnS–5%GR electrode, which is shown in Figure S4 (Supporting Information). In contrast, for blank ZnS under visible light irradiation, no photocurrent is observed with the switch-on and switch-off cycles. We have also performed the photoluminescent (PL) spectroscopy measurement of blank ZnS and commercial ZnS samples, which have different particle sizes (Figure S5, Supporting Information), under visible light excitation. No PL emission signal is observed for ZnS samples under visible light excitation (Figure S6, Supporting Information). Thus, it is clear that ZnS with different particle sizes is not able to reach excited states under visible light irradiation. Interestingly, for ZnS–5%GR under visible light irradiation, a peak ranging from 500 to 600 nm is observed (Figure S7, Supporting Information), which can be ascribed to the PL emission signal from GR in ZnS–5%GR under visible light excitation. This observation suggests that, under visible light irradiation, GR in the ZnS–5%GR nanocomposite can be excited from ground state GR to excited state GR*, which then acts as a macromolecular photosensitizer for ZnS. As a result, ZnS–5%GR is able to show visible light

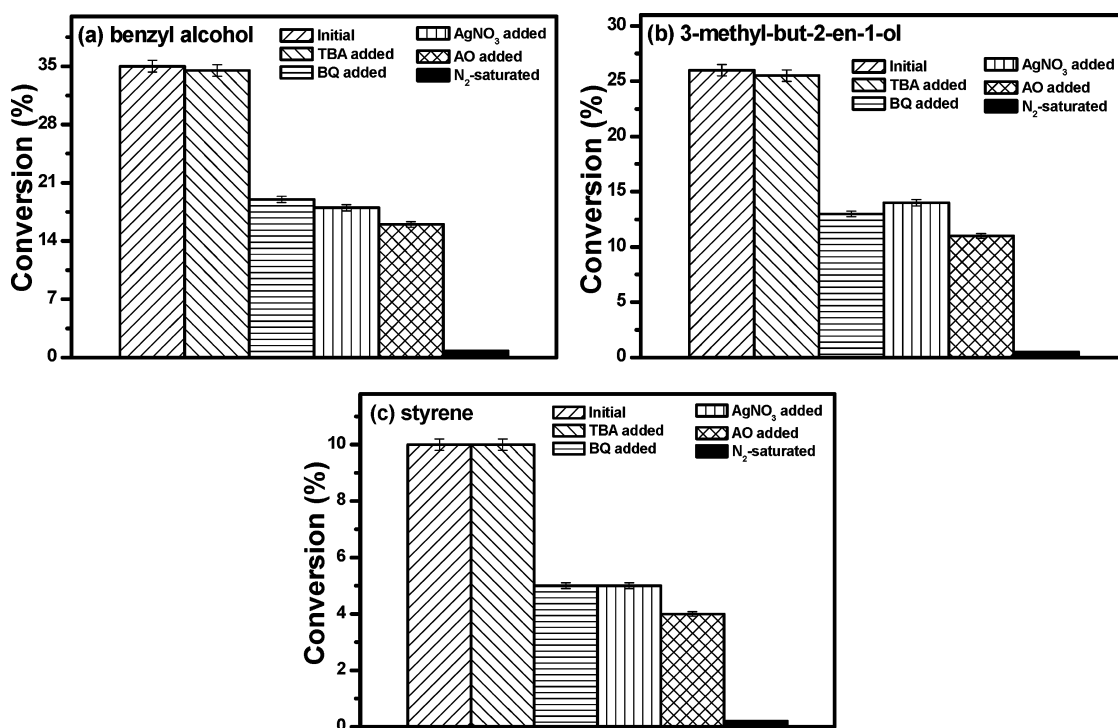


Figure 9. Controlled experiments of photocatalytic selective oxidation of benzyl alcohol (a), 3-methylbut-2-en-1-ol (b), and styrene (c) in the presence of *tert*-butyl alcohol (TBA, scavenger for hydroxyl radicals), benzoquinone (BQ, scavenger for superoxide radicals), AgNO₃ (scavenger for electrons), ammonium oxalate (AO, scavenger for holes), or N₂-saturated condition over the optimum ZnS–5%GR under UV light ($\lambda = 350 \pm 15$ nm) irradiation for 4 h.

photoactivity toward oxidation of alcohols and alkenes as discussed above. These results further evidence that the coupling of ZnS with GR by a good interfacial contact significantly facilitates the charge carrier transfer process upon visible light irradiation, and the role of GR vividly acts as a macromolecular photosensitizer.

The quantum confinement effect can also be excluded as the possible factor leading to the as-observed photoactivity for the ZnS–5%GR nanocomposite under visible light irradiation. It is well-known that the optical and electronic properties for nanostructured materials with small size, typically at the nanoscale, often exhibit the quantum confinement phenomenon. As a result, the band gap becomes size-dependent, which ultimately results in a blue shift (*i.e.*, increased band gap) in optical illumination as the size of the particles decreases. Thus, the smaller size of ZnS nanoparticles cannot be the reason for the as-observed photoactivity of ZnS–5%GR under visible light irradiation. As mentioned above, under visible light excitation, there is no PL signal observed for blank ZnS, which has similar particle sizes as that for ZnS in ZnS–5%GR. This suggests that, under visible light irradiation, ZnS is not able to reach excited states.

The GR-induced photosensitization mechanism for ZnS–5%GR under visible light irradiation can also be further corroborated by the photoactivity test under UV light irradiation ($\lambda = 350 \pm 15$ nm). When the reaction is performed under UV light irradiation, the

incident photon energy can promote the band gap excitation of ZnS, by which the electron–hole ($h^+ - e^-$) pairs can be generated. As we know, the positive holes generally have strong oxidation power that is able to boost the efficiency for the photocatalytic oxidation reaction,^{45,51} thus leading to higher photoactivity. As expected (Figure S8, Supporting Information), the photoactivity is improved obviously for ZnS–5%GR under UV light irradiation as compared to that under visible light irradiation. In particular, as displayed in Figure 9, controlled experiments using different radical scavengers under UV light irradiation provide us with a detailed mechanism message on the role of photo-activated species, which is remarkably different from that under visible light irradiation. It can be seen that, under UV light irradiation, the addition of the AO scavenger for holes plays an obvious inhibition effect on conversion of substrate reactants including benzyl alcohol (a), 3-methylbut-2-en-1-ol (b), or styrene (c) in Figure 9, suggesting that the positive holes, photo-generated from band gap excitation of ZnS, involve the oxidation of alcohol or alkene. This phenomenon is distinctly different from the case for ZnS–5%GR under visible light irradiation, for which no positive holes can be generated, and thus we do not observe the inhibition effect on conversion of alcohol or alkene when adding AO into the reaction system, as shown in Figure 8. In addition, it should be noted that, under UV light irradiation, the degree of inhibition effect on

the reaction resulting from the addition of electron and superoxide radical scavengers (AgNO_3 and BQ, respectively) is obviously lower than that under visible light irradiation. This observation is reasonable because, under UV light irradiation, the positive holes generated from band gap excitation of ZnS also participate in the oxidation reaction; however, under visible light irradiation, only the electrons photogenerated from GR are the primary active species that are able to activate molecular oxygen. In other words, for the oxidation reaction over ZnS–5%GR under UV light irradiation, the primary active species are holes, electrons, and activated oxygen (e.g., superoxide radicals), which together account for the oxidation of substrate alcohols or alkenes. For the case of ZnS–5%GR under visible light irradiation, the oxidation reaction is mainly initiated by the photoexcited electrons from GR under visible light irradiation, that is, a GR-photosensitized photocatalytic process as mentioned above.

In addition, in order to learn if the interfacial contact between GR and ZnS plays an important effect on observing the photosensitizer role of GR for semiconductor ZnS, we have also tested the photocatalytic performance of the ZnS–5%GR nanocomposite that is prepared by a simple mechanical mixing of blank ZnS and GR. The results show that ZnS–5%GR obtained by a mechanical mixing method exhibits very poor photoactivity toward selective oxidation of alcohols or alkenes, which is similar to the case for the blank ZnS sample. Furthermore, we have considered the effect of reduction degree of GO on the photocatalytic performance of ZnS–5%GR under visible light irradiation. It can be seen from Figure S9 that a sufficient reduction of GO to GR also plays a significant role in determining the photoactivity of ZnS–5%GR. Therefore, these results suggest that the intimate interfacial interaction between ZnS and GR and the sufficient reduction of GO to GR are two key factors resulting in (a) the efficient charge carrier transfer along the interface between ZnS and GR, and (b) GR efficiently acting as a macromolecular photosensitizer for semiconductor ZnS under visible light irradiation.

Thus far, the photocatalytic process for ZnS–5%GR under visible light irradiation seems to be very similar to the well-known strategy of photosensitization of semiconductors (e.g., TiO_2) by the matched adsorption of organic dyes, by which the photoresponse of a wide band gap semiconductor can be extended to the visible light region. The photocatalytic process resulting from a dye-sensitized semiconductor under visible light irradiation generally includes the following steps: (a) dye excitation upon visible light irradiation, (b) electron injection into the conduction band (CB) of the semiconductor, (c) trapping the injected electrons by surface sites, (d) scavenging electrons in the CB of the semiconductor by electron acceptors such as O_2 , and (e) subsequent radical reactions. During

the whole process, because the semiconductor is not able to be band-gap-photoexcited, no holes are involved.⁴⁴

The above discussion leads us to conclude that the photoactive species for photocatalytic aerobic oxidation of alcohols and alkenes for ZnS–5%GR under visible light irradiation does not originate from the “electron–hole” pairs because, under visible light irradiation, wide band gap ZnS is not able to be band-gap-photoexcited. Also, ZnS cannot reach excited states under visible light irradiation. On the contrary, it should be understood by an organic dye-like photosensitization process. In other words, GR acts as an organic dye-like macromolecular photosensitizer in the nanocomposite of ZnS–5%GR. Under visible light irradiation, GR is photoexcited from the ground state to excited state, namely, from GR to GR^* , which is similar to the photoexcitation of organic dyes adsorbed on the semiconductor.⁴⁴ GR^* in the excited state injects electrons into the conduction band of ZnS. Electrons can be trapped by molecular oxygen in the reaction system by which oxygen is activated; for example, superoxide radicals can be formed (Figure S3, Supporting Information). The adsorbed alcohols or alkenes over the surface of ZnS–5%GR are oxidized by activated oxygen to give rise to target products, corresponding aldehydes, or epoxides. Such a novel photocatalytic mechanism is remarkably different from previous research works regarding all other GR–semiconductor photocatalysts, for which GR is proposed to behave as an electron reservoir to capture the electrons photogenerated from the semiconductor.^{1–37} To the best of our knowledge, this is the first direct and robust experimental evidence to show the role of GR as a photosensitizer for transforming the only UV light photoactive semiconductor to the visible light photocatalyst used for a selective oxidation reaction under ambient conditions.

CONCLUSIONS

In summary, a series of ZnS–GR nanocomposites with different weight addition ratios of GR have been fabricated *via* a facile two-step wet chemistry method. The ZnS–GR nanocomposites can serve as a visible light photocatalyst toward selective aerobic oxidation of alcohols and alkenes under ambient conditions. It has been demonstrated for the first time that the visible-light-driven photocatalytic aerobic oxidation process for ZnS–GR results from a GR photosensitization of ZnS, for which upon visible light irradiation no holes are generated because the wide band gap of ZnS is not able to be photoexcited by visible light irradiation. This novel photocatalytic mechanism is totally different from all other reported GR–semiconductor photocatalysts, for which GR is always claimed to behave as an electron reservoir to capture/shuttle the electrons photogenerated from semiconductor.

Overall, it is hoped that our findings of the novel role of GR as a “photosensitizer” in ZnS–GR nanocomposites may offer a new useful guide for designing GR–semiconductor composite photocatalysts toward

selective transformations and importantly promote our in-depth thinking on the exact microscopic charge carrier transfer pathway along the interface between the GR sheet and the semiconductor.

METHODS

Synthesis. Graphene oxide (GO), the precursor of graphene (GR) in this work, was prepared by a modified Hummers method, which was also used in our previous studies.^{8,19} Detailed synthesis details of GO, atomic force microscopy (AFM) images, and height profiles of GO are provided in the Supporting Information. The synthesis of ZnS–GR nanocomposites with different weight addition ratios of GR was typically performed as follows. GO was dispersed into 50 mL of deionized water completely by ultrasonication, and then 10 mL of 0.15 M ZnCl₂ solution was added and this suspension was heated to 333 K in an oil bath with magnetic stirring for 2 h. During this step, the positively charged Zn²⁺ can be adsorbed onto the negatively charged GO surface by the electrostatic attraction. Subsequently, 20 mL of 0.10 M Na₂S solution was added drop by drop and kept stirring for 4 h, which allows the formation of ZnS nanoparticles on the GO platform. Then, it was transferred to a 100 mL Teflon-sealed autoclave and maintained at 403 K for 12 h, which allows sufficient reduction of GO to GR. Next, the products were cooled to room temperature and recovered by filtration, washed by water, and fully dried at 333 K in an oven to obtain the final ZnS–GR nanocomposites with different weight addition ratios of GR, namely, 1, 5, 10, and 30%GR–ZnS nanocomposites. For comparison, blank ZnS was prepared using the same procedures in the absence of GO.

Characterization. The crystalline structure of the samples was determined by the powder X-ray diffraction (XRD), using Ni-filtered Cu K α radiation in the 2 θ range from 5 to 80° with a scan rate of 0.08° per second. The optical properties of the samples were analyzed by the UV–vis diffuse reflectance spectroscopy (DRS) using a Cary-500 spectrophotometer over a wavelength range of 250–800 nm, during which BaSO₄ was employed as the internal reflectance standard. The morphology and microscopic structure information were determined by field-emission scanning electron microscopy (FESEM, FEI Nova NANOSEM 230) and transmission electron microscopy (TEM, FEI Tecnai G2 F20 S-TWIN), respectively. Tapping-mode atomic force microscopy (AFM) measurements were performed on a Nanoscope IIIA system. The sample for AFM imaging was prepared by depositing suspensions of graphene oxide (GO) in ethanol on a freshly cleaved mica surface. For the TEM analysis, the samples were dispersed in ethanol by ultrasonic treatment and dropped on the lacey support film without carbon-coated copper grids. Raman spectroscopic measurements were performed on a Renishaw inVia Raman System 1000 with a 532 nm Nd:YAG excitation source at room temperature. The photoluminescence (PL) spectra were obtained using an Edinburgh Analytical Instrument PLS920 system. The Fourier transformed infrared spectroscopy (FTIR) was performed on a Nicolet Nexus 670 FTIR spectrophotometer at a resolution of 4 cm^{−1}.

The electron spin resonance (ESR) spectra of the radical species that are spin-trapped by 5,5-dimethyl-1-pyrroline-N-oxide (DMPO) were measured using a Bruker EPR A300 spectrometer. The as-prepared sample powder (5 mg) was dispersed in 0.5 mL of benzotrifluoride (BTF). Then, 25 μ L of DMPO/benzyl alcohol solution (1:10, v/v) was added and oscillated to achieve the well-blended suspension. The irradiation source ($\lambda > 420$ nm) was a 300 W Xe arc lamp system, the very light source for our photocatalytic selective oxidation experiments as shown below. The settings for the ESR spectrometer were as follows: center field = 3507 G, microwave frequency = 9.84 GHz, and power = 6.36 mW.

Photoelectrochemical measurements were performed in a homemade three-electrode quartz cell with a BAS Epsilon workstation without bias. Pt plate was used as counter and

Ag/AgCl electrode used as reference electrodes, while the working electrode was prepared on fluoride–tin oxide (FTO) conductor glass. The sample powder (10 mg) was ultrasonicated in 1 mL of anhydrous ethanol to disperse it evenly to get a slurry. The slurry was spread onto an FTO glass whose side was previously protected using Scotch tape. The working electrode was dried under ambient conditions. Uncoated parts of the electrode were isolated with epoxy resin. The electrolyte was 0.2 M aqueous Na₂SO₄ solution (pH = 6.8) without additive. The visible light irradiation source was a 300 W Xe lamp system equipped with a UV cutoff filter ($\lambda > 420$ nm).

Photoactivity. Photocatalytic selective oxidation of organic compounds (alcohols or alkenes) was performed in a 10 mL Pyrex glass bottle under the irradiation of visible light.^{19,20} In a typical process, a mixture of catalyst (8 mg) and organic compounds (0.1 mmol) was dissolved in the solvent (1.5 mL) of benzotrifluoride (BTF), which was saturated with pure molecular oxygen (purity >99.99%) from a gas cylinder. The above mixture was transferred into a 10 mL Pyrex glass bottle and stirred for 10 min to make the catalyst blend evenly in the solution. The suspensions were irradiated by a 300 W Xe arc lamp (PLS-SXE 300, Beijing Perfectlight Co. Ltd.) with a UV cutoff filter ($\lambda > 420$ nm). After the reaction, the mixture was centrifuged at 12 000 rpm for 20 min to completely remove the catalyst particles. The remaining solution was analyzed with an Agilent gas chromatograph (GC-7820 fitted with a FFAP capillary analysis column). The assignment of products was confirmed by a Hewlett-Packard gas chromatograph/mass spectrometer (HP-5973GC/MS). Controlled photoactivity experiments using different radical scavengers (ammonium oxalate as scavenger for photogenerated holes, AgNO₃ as scavenger for electrons, benzoquinone as scavenger for superoxide radical species, and *tert*-butyl alcohol for hydroxyl radical species) were performed similar to the above photocatalytic oxidation of alcohol or alkene except that the radical scavengers (0.1 mmol) were added to the reaction system.^{45–50} Conversion, yield, and selectivity for selective oxidation of organic compounds to target product were defined as follows:

$$\text{conversion (\%)} = [(C_0 - C_t)/C_0] \times 100$$

$$\text{yield (\%)} = C_p/C_0 \times 100$$

$$\text{selectivity (\%)} = [C_p/(C_0 - C_t)] \times 100$$

where C_0 is the initial concentration of alcohols or alkenes and C_t and C_p are the concentration of reactant and product, respectively, at a certain time after the photocatalytic reaction.

Conflict of Interest: The authors declare no competing financial interest.

Acknowledgment. The support by the National Natural Science Foundation of China (NSFC) (21173045, 20903022, 20903023), the Award Program for Minjiang Scholar Professorship, the Natural Science Foundation (NSF) of Fujian Province for Distinguished Young Investigator Grant (2012J06003), Program for Changjiang Scholars and Innovative Research Team in Universities (PCSIRT0818), Program for Returned High-Level Overseas Chinese Scholars of Fujian Province, and the Project Sponsored by the Scientific Research Foundation for the Returned Overseas Chinese Scholars, State Education Ministry, is gratefully acknowledged.

Supporting Information Available: Fourier transformed infrared spectra (FTIR) of the ZnS–5%GR nanocomposite and the

original graphene oxide (GO) sample; photographs of the samples of blank ZnS and ZnS–GR nanocomposites; ESR spectra of DMPO–O₂^{•−} adduct in the blank ZnS and ZnS–5%GR; photocurrent transient responses of blank ZnS and ZnS–5%GR electrodes; SEM images of blank ZnS and commercial ZnS and their size distribution; photoluminescent spectra of blank ZnS, commercial ZnS, and ZnS–5%GR excited at 420 nm; photoactivity test over ZnS–5%GR under UV light ($\lambda = 350 \pm 15$ nm) and visible light ($\lambda > 420$ nm) irradiation; the effect of hydrothermal treatment time on the photoactivity of oxidation of benzyl alcohol to benzaldehyde over ZnS–5%GR under visible light irradiation ($\lambda > 420$ nm); experimental details for synthesis of GO; AFM image and height profiles of GO. This material is available free of charge via the Internet at <http://pubs.acs.org>.

REFERENCES AND NOTES

- Lightcap, I. V.; Kosel, T. H.; Kamat, P. V. Anchoring Semiconductor and Metal Nanoparticles on a Two-Dimensional Catalyst Mat. Storing and Shuttling Electrons with Reduced Graphene Oxide. *Nano Lett.* **2010**, *10*, 577–583.
- Kamat, P. V. Graphene-Based Nanoassemblies for Energy Conversion. *J. Phys. Chem. Lett.* **2011**, *2*, 242–251.
- An, X.; Yu, J. C. Graphene-Based Photocatalytic Composites. *RSC Adv.* **2011**, *1*, 1426–1434.
- Huang, X.; Qi, X.; Boey, F.; Zhang, H. Graphene-Based Composites. *Chem. Soc. Rev.* **2012**, *41*, 666–686.
- Zhang, N.; Zhang, Y.; Xu, Y.-J. Recent Progress on Graphene-Based Photocatalysts: Current Status and Future Perspectives. *Nanoscale* **2012**, *4*, 5792–5813.
- Xiang, Q.; Yu, J.; Jaroniec, M. Graphene-Based Semiconductor Photocatalysts. *Chem. Soc. Rev.* **2012**, *41*, 782–796.
- Chen, C.; Cai, W.; Long, M.; Zhou, B.; Wu, Y.; Wu, D.; Feng, Y. Synthesis of Visible-Light Responsive Graphene Oxide/TiO₂ Composites with p/n Heterojunction. *ACS Nano* **2010**, *4*, 6425–6432.
- Zhang, Y.; Tang, Z.-R.; Fu, X.; Xu, Y.-J. TiO₂-Graphene Nanocomposites for Gas-Phase Photocatalytic Degradation of Volatile Aromatic Pollutant: Is TiO₂-Graphene Truly Different from Other TiO₂-Carbon Composite Materials? *ACS Nano* **2010**, *4*, 7303–7314.
- Zhang, H.; Lv, X.; Li, Y.; Wang, Y.; Li, J. P25-Graphene Composite as a High Performance Photocatalyst. *ACS Nano* **2010**, *4*, 380–386.
- Zhang, J.; Xiong, Z.; Zhao, X. S. Graphene-Metal-Oxide Composites for the Degradation of Dyes under Visible Light Irradiation. *J. Mater. Chem.* **2011**, *21*, 3634–3640.
- Fan, W.; Lai, Q.; Zhang, Q.; Wang, Y. Nanocomposites of TiO₂ and Reduced Graphene Oxide as Efficient Photocatalysts for Hydrogen Evolution. *J. Phys. Chem. C* **2011**, *115*, 10694–10701.
- Xu, T.; Zhang, L.; Cheng, H.; Zhu, Y. Significantly Enhanced Photocatalytic Performance of ZnO via Graphene Hybridization and the Mechanism Study. *Appl. Catal., B* **2011**, *101*, 382–387.
- Li, Q.; Guo, B.; Yu, J.; Ran, J.; Zhang, B.; Yan, H. J.; Gong, J. R. Highly Efficient Visible-Light-Driven Photocatalytic Hydrogen Production of CdS-Cluster-Decorated Graphene Nanosheets. *J. Am. Chem. Soc.* **2011**, *133*, 10878–10884.
- Ng, Y. H.; Lightcap, I. V.; Goodwin, K.; Matsumura, M.; Kamat, P. V. To What Extent Do Graphene Scaffolds Improve the Photovoltaic and Photocatalytic Response of TiO₂ Nanostructured Films? *J. Phys. Chem. Lett.* **2010**, *1*, 2222–2227.
- Zhang, X.-Y.; Li, H.-P.; Cui, X.-L.; Lin, Y. Graphene/TiO₂ Nanocomposites: Synthesis, Characterization and Application in Hydrogen Evolution from Water Photocatalytic Splitting. *J. Mater. Chem.* **2010**, *20*, 2801–2806.
- Akhavan, O.; Ghaderi, E. Photocatalytic Reduction of Graphene Oxide Nanosheets on TiO₂ Thin Film for Photo-inactivation of Bacteria in Solar Light Irradiation. *J. Phys. Chem. C* **2009**, *113*, 20214–20220.
- Akhavan, O. Graphene Nanomesh by ZnO Nanorod Photocatalysts. *ACS Nano* **2010**, *4*, 4174–4180.
- Iwase, A.; Ng, Y. H.; Ishiguro, Y.; Kudo, A.; Amal, R. Reduced Graphene Oxide as a Solid-State Electron Mediator in Z-Scheme Photocatalytic Water Splitting under Visible Light. *J. Am. Chem. Soc.* **2011**, *133*, 11054–11057.
- Zhang, Y.; Tang, Z.-R.; Fu, X.; Xu, Y.-J. Engineering the Unique 2D Mat of Graphene To Achieve Graphene-TiO₂ Nanocomposite for Photocatalytic Selective Transformation: What Advantage Does Graphene Have over Its Forebear Carbon Nanotube? *ACS Nano* **2011**, *5*, 7426–7435.
- Zhang, Y.; Zhang, N.; Tang, Z.-R.; Xu, Y.-J. Improving the Photocatalytic Performance of Graphene of Graphene-TiO₂ Nanocomposites via a Combined Strategy of Decreasing Defects of Graphene and Increasing Interfacial Contact. *Phys. Chem. Chem. Phys.* **2012**, *14*, 9167–9175.
- Liang, Y. T.; Vijayan, B. K.; Gray, K. A.; Hersam, M. C. Minimizing Graphene Defects Enhances Titania Nanocomposite-Based Photocatalytic Reduction of CO₂ for Improved Solar Fuel Production. *Nano Lett.* **2011**, *11*, 2865–2870.
- Liang, Y. T.; Vijayan, B. K.; Lyandres, O.; Gray, K. A.; Hersam, M. C. Effect of Dimensionality on the Photocatalytic Behavior of Carbon-Titania Nanosheet Composites: Charge Transfer at Nanomaterial Interfaces. *J. Phys. Chem. Lett.* **2012**, *3*, 1760–1765.
- Akhavan, O.; Choobtashani, M.; Ghaderi, E. Protein Degradation and RNA Efflux of Viruses Photocatalyzed by Graphene-Tungsten Oxide Composite under Visible Light Irradiation. *J. Phys. Chem. C* **2012**, *116*, 9653–9659.
- Ng, Y. H.; Iwase, A.; Kudo, A.; Amal, R. Reducing Graphene Oxide on a Visible-Light BiVO₄ Photocatalyst for an Enhanced Photoelectrochemical Water Splitting. *J. Phys. Chem. Lett.* **2010**, *1*, 2607–2612.
- Ai, Z.; Ho, W.; Lee, S. Efficient Visible Light Photocatalytic Removal of NO with BiOBr-Graphene Nanocomposites. *J. Phys. Chem. C* **2011**, *115*, 25330–25337.
- Min, Y.-L.; Zhang, K.; Chen, Y.-C.; Zhang, Y.-G. Enhanced Photocatalytic Performance of Bi₂WO₆ by Graphene Supporter as Charge Transfer Channel. *Sep. Purif. Technol.* **2012**, *86*, 98–105.
- Williams, G.; Kamat, P. V. Graphene-Semiconductor Nanocomposites: Excited-State Interactions between ZnO Nanoparticles and Graphene Oxide. *Langmuir* **2009**, *25*, 13869–13873.
- Luo, Q.-P.; Yu, X.-Y.; Lei, B.-X.; Chen, H.-Y.; Kuang, D.-B.; Su, C.-Y. Reduced Graphene Oxide-Hierarchical ZnO Hollow Sphere Composites with Enhanced Photocurrent and Photocatalytic Activity. *J. Phys. Chem. C* **2012**, *116*, 8111–8117.
- Fu, Y.; Xiong, P.; Chen, H.; Sun, X.; Wang, X. High Photocatalytic Activity of Magnetically Separable Manganese Ferrite-Graphene Heteroarchitectures. *Ind. Eng. Chem. Res.* **2012**, *51*, 725–731.
- Williams, G.; Seger, B.; Kamat, P. V. TiO₂-Graphene Nanocomposites. UV-Assisted Photocatalytic Reduction of Graphene Oxide. *ACS Nano* **2008**, *2*, 1487–1491.
- Du, J.; Lai, X.; Yang, N.; Zhai, J.; Kisailus, D.; Su, F.; Wang, D.; Jiang, L. Hierarchically Ordered Macro-Mesoporous TiO₂-Graphene Composite Films: Improved Mass Transfer, Reduced Charge Recombination, and Their Enhanced Photocatalytic Activities. *ACS Nano* **2011**, *5*, 590–596.
- Jiang, B.; Tian, C.; Pan, Q.; Jiang, Z.; Wang, J.-Q.; Yan, W.; Fu, H. Enhanced Photocatalytic Activity and Electron Transfer Mechanisms of Graphene/TiO₂ with Exposed {001} Facets. *J. Phys. Chem. C* **2011**, *115*, 23718–23725.
- Hayashi, H.; Lightcap, I. V.; Tsujimoto, M.; Takano, M.; Umeyama, T.; Kamat, P. V.; Imahori, H. Electron Transfer Cascade by Organic/Inorganic Ternary Composites of Porphyrin, Zinc Oxide Nanoparticles, and Reduced Graphene Oxide on a Tin Oxide Electrode That Exhibits Efficient Photocurrent Generation. *J. Am. Chem. Soc.* **2011**, *133*, 7684–7687.
- Mukherji, A.; Seger, B.; Lu, G. Q.; Wang, L. Nitrogen Doped Sr₂Ta₂O₇ Coupled with Graphene Sheets as Photocatalysts for Increased Photocatalytic Hydrogen Production. *ACS Nano* **2011**, *5*, 3483–3492.

35. Xiang, Q.; Yu, J.; Jaroniec, M. Enhanced Photocatalytic H₂-Production Activity of Graphene-Modified Titania Nanosheets. *Nanoscale* **2011**, *3*, 3670–3678.
36. Chen, P.; Xiao, T.-Y.; Li, H.-H.; Yang, J.-J.; Wang, Z.; Yao, H.-B.; Yu, S.-H. Nitrogen-Doped Graphene/ZnSe Nanocomposites: Hydrothermal Synthesis and Their Enhanced Electrochemical and Photocatalytic Activities. *ACS Nano* **2012**, *6*, 712–719.
37. Hu, H.; Wang, X.; Liu, F.; Wang, J.; Xu, C. Rapid Microwave-Assisted Synthesis of Graphene Nanosheets-Zinc Sulfide Nanocomposites: Optical and Photocatalytic Properties. *Synth. Met.* **2011**, *161*, 404–410.
38. Du, A.; Ng, Y. H.; Bell, N. J.; Zhu, Z.; Amal, R.; Smith, S. C. Hybrid Graphene/Titania Nanocomposite: Interface Charge Transfer, Hole Doping, and Sensitization for Visible Light Response. *J. Phys. Chem. Lett.* **2011**, *2*, 894–899.
39. Nethravathi, C.; Rajamathi, M. Chemically Modified Graphene Sheets Produced by the Solvothermal Reduction of Colloidal Dispersions of Graphite Oxide. *Carbon* **2008**, *46*, 1994–1998.
40. Woan, K.; Pyrgiotakis, G.; Sigmund, W. Photocatalytic Carbon-Nanotube-TiO₂ Composites. *Adv. Mater.* **2009**, *21*, 2233–2239 and references therein.
41. Leary, R.; Westwood, A. Carbonaceous Nanomaterials for the Enhancement of TiO₂ Photocatalysis. *Carbon* **2011**, *49*, 741–772 and references therein.
42. Kamat, P. V.; Gevaert, M.; Vinodgopal, K. Photochemistry on Semiconductor Surface. Visible Light Induced Oxidation of C₆₀ on TiO₂ Nanoparticles. *J. Phys. Chem. B* **1997**, *101*, 4422–4427.
43. Wang, W.; Serp, P.; Kalck, P.; Faria, J. L. Visible Light Photodegradation of Phenol on MWNT-TiO₂ Composite Catalysts Prepared by a Modified Sol–Gel Method. *J. Mol. Catal., A* **2005**, *235*, 194–199.
44. Chen, C.; Ma, W.; Zhao, J. Semiconductor-Mediated Photodegradation of Pollutants under Visible-Light Irradiation. *Chem. Soc. Rev.* **2010**, *39*, 4206–4219 and references therein.
45. Zhang, Y.; Zhang, N.; Tang, Z.-R.; Xu, Y.-J. Transforming CdS into an Efficient Visible Light Photocatalyst for Selective Oxidation of Saturated Primary C–H Bonds under Ambient Conditions. *Chem. Sci.* **2012**, *3*, 2812–2822.
46. Carp, O.; Huisman, C. L.; Reller, A. Photoinduced Reactivity of Titanium Dioxide. *Prog. Solid State Chem.* **2004**, *32*, 33–177.
47. Li, W.; Li, D.; Lin, Y.; Wang, P.; Chen, W.; Fu, X.; Shao, Y. Evidence for the Active Species Involved in the Photodegradation Process of Methyl Orange on TiO₂. *J. Phys. Chem. C* **2012**, *116*, 3552–3560.
48. Zhang, N.; Liu, S.; Fu, X.; Xu, Y.-J. Synthesis of M@TiO₂ (M = Au, Pd, Pt) Core–Shell Nanocomposites with Tunable Photoreactivity. *J. Phys. Chem. C* **2011**, *115*, 9136–9145.
49. Stylidi, M.; Kondarides, D. I.; Verykios, X. E. Visible Light-Induced Photocatalytic Degradation of Acid Orange 7 in Aqueous TiO₂ Suspensions. *Appl. Catal., B* **2004**, *47*, 189–201.
50. Raja, P.; Bozzi, A.; Mansilla, H.; Kiwi, J. Evidence for Superoxide-Radical Anion, Singlet Oxygen and OH-Radical Intervention during the Degradation of Lignin Model Compound (3-Methoxy-4-Hydroxyphenylmethylcarbinol). *J. Photochem. Photobiol., A* **2005**, *169*, 271–278.
51. Maldotti, A.; Molinari, A.; Amadelli, R. Photocatalysis with Organized Systems for the Oxofunctionalization of Hydrocarbons by O₂. *Chem. Rev.* **2002**, *102*, 3811–3836.